Transition between curved and angular textures in binary fluid convection

A. La Porta, K. D. Eaton, and C. M. Surko
Department of Physics, University of California, San Diego, La Jolla, California 92093
(Received 25 September 1995)

We report a transition from a curved texture to an angular texture in Rayleigh-Bénard convection in a mixture of ethanol and water. The transition occurs as the Rayleigh number is reduced from a high value and approaches the traveling-wave branch and is observed at negative values of the separation ratio in fluid mixtures, but not in a pure fluid. We show that this transition may be understood in terms of a generalization of the Swift-Hohenberg free energy functional. A large increase in wave-number rigidity is observed as the traveling-wave transition is approached.

PACS number(s): 47.54.+r, 47.20.Lz, 47.27.Te

I. INTRODUCTION

Pattern formation in nonequilibrium systems is of fundamental interest because no general theory is known which governs these systems and because, in many instances, striking similarities are observed between patterns produced by different physical mechanisms, suggesting that common organizing principles are at work [1,2]. The search for such universal aspects of patterns is one of the primary goals of the field. Rayleigh-Bénard convection has been one of the most widely studied pattern forming systems because the physical mechanisms involved are well understood, precise control of experimental parameters is possible, and a great variety of phenomena can be observed and studied. In this paper, we describe a previously unreported transition in the texture of convection patterns. This transition, which occurs in convection in a binary mixture, is from a curved texture, which is generic to Rayleigh-Bénard convection, to an angular texture, in which patches of straight rolls are connected by sharp domain boundaries. The formation of the angular texture is coincident with the transition from stationary convection to traveling-wave convection in the mixture. We show that this transition can be described by defining a free energy functional that is minimized by the selected pattern, and whose form is a generalization of that calculated from the Swift-Hohenberg model [3,4]. The angular patterns that are observed are very similar to the labyrinth patterns observed in ferromagnetic garnet films [5], and so this transition and its mathematical description appear to bridge the gap between typical convection patterns and the labyrinth patterns. In addition, the formation of the angular texture, which does not occur in the standard Swift-Hohenberg model, gives additional information about the nature of the bifurcation from stationary to traveling waves.

II. TRAVELING-WAVE AND STATIONARY CONVECTION IN FLUID MIXTURES

Rayleigh-Bènard convection in a binary mixture is primarily studied as a system that supports oscillatory and traveling-wave (TW) convection. In fluid mixtures of ethanol and water, there is a strong Soret effect in which the diffusion of ethanol in the fluid is driven by a temperature gradient. For ethanol concentrations of less than 26%, the Soret coefficient is negative, and ethanol is driven towards the colder regions of the convection cell. As a result, when the convection cell is heated from below, the accumulation of ethanol at the top of the cell tends to stabilize the fluid layer against thermal convection. This competition between thermal and concentration effects results in a suppression of the onset of convection compared with a pure fluid and, depending on the system parameters, oscillatory convection, traveling-wave convection, or stationary overturning convection (SOC) can occur [2,6].

Binary fluid convection is described by four dimensionless numbers. The forcing parameter is the Rayleigh number,

$$\mathrm{Ra} = \frac{\alpha g h^3 \Delta T}{\kappa \nu}, \tag{1}$$

where α is the thermal expansion coefficient, g is the acceleration of gravity, κ is the thermal diffusion constant, and ν is the viscosity. It is convenient to use the reduced Rayleigh number, $r = \mathrm{Ra}/1708$, which is normalized to the onset of convection in a pure fluid. The Prandtl number,

$$\mathrm{Pr} = \frac{\nu}{\kappa}, \tag{2}$$

determines the onset of secondary instabilities and influences the nature of the patterns. The separation ratio,

$$\psi = c\,(1-c)\,S_t \frac{\beta}{\alpha}, \tag{3}$$

where S_t is the Soret coefficient and β is the concentration expansion coefficient, indicates the extent to which the ethanol concentration of the fluid layer is stratified in response to a temperature gradient, and the Lewis number,

$$\mathcal{L} = \frac{D_c}{\kappa}, \tag{4}$$

where D_c is the mass diffusion coefficient for ethanol, gives the ratio of the time scales for mass and thermal diffusion.

In the ethanol-water mixture, $\mathcal{L} \approx 10^{-2}$, so there is a strong separation of the diffusive time scales and within experimental accuracy, a TW state is observed for all $\psi < 0$. In Fig. 1, the bifurcation diagram is sketched for a pure fluid and for fluid mixtures with two different values of ψ. The primary results presented below were obtained using a mixture of 8% ethanol (by weight) in water at an average temperature of 26 °C, which has a large negative separation ratio, $\psi = -0.24$, and for which Pr = 10.5. For this value of ψ, the onset of convection is strongly subcritical, and the first bifurcation, at r_{co}, is a Hopf bifurcation to a state of oscillatory convection that grows until a large amplitude state of traveling-wave convection is reached. If the Rayleigh number is increased further, the traveling-wave velocity goes to zero at r^*, and if the Rayleigh number is decreased, TW convection persists until a saddle node bifurcation is encountered at r_s. The texture transition studied below occurs above r^*, where stationary overturning convection (SOC) is observed. At these high values of the Rayleigh number, the variation in ethanol concentration is strongly suppressed by the vigorous convective flow, and previous work on two-dimensional convection indicated that in this regime, the mixture behaves like a pure fluid [7–9]. The present experiment suggests that concentration effects are still important above r^* in the presence of three-dimensional flow effects, which are important near defects in the pattern. For comparison, data is also shown that was obtained from a mixture of 1% ethanol in water, for which $\psi = -0.06$ and Pr = 6.5. The behavior of the 1% mixture is qualitatively the same as that of the 8% mixture, although the range over which TW convection is observed is much smaller and the TW state has a smaller amplitude (see Fig. 1).

III. OBSERVATION OF THE TRANSITION

The patterns are observed in a cylindrical convection cell with a height of 0.4 cm and a radius of 10.5 cm.

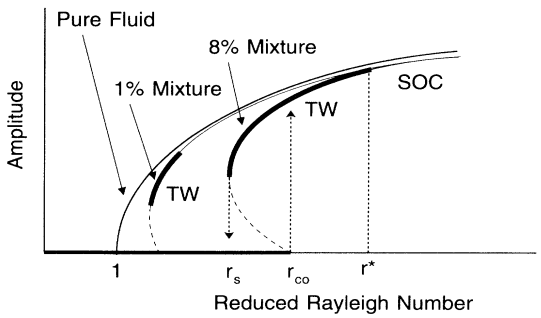

FIG. 1. Schematic bifurcation diagram for convection in pure water and in binary mixtures containing 8% ethanol by weight (for which $\psi = -0.24$) and 1% ethanol by weight (for which $\psi = -0.06$). For each mixture the regime of TW convection is indicated by a thick line, and the bifurcation points are indicated for the 8% mixture.

The upper boundary is a sapphire disk that is maintained at 25 °C by a temperature regulated flow bath, and the lower boundary is a solid silicon disk that is electrically heated to produce a temperature difference of 2–5 °C. The convection cell is visualized through the upper boundary by a white light shadowgraph and convection patterns are recorded using a charge-coupled-device camera. Images with a spatial resolution of 480 × 480 are acquired at eight-bit accuracy using a personal computer frame grabber and stored in binary computer files.

In order to measure the local properties of the convection patterns, the digitized shadowgraph images are divided by a reference image of the convection cell, below the threshold of convection, in order to compensate for nonuniformity of illumination. The image is then convoluted with a Gaussian function having a standard deviation equal to about half of the width of a convection roll in order to suppress broadband noise. The gradient of the filtered images is perpendicular to the roll boundaries, and can be used to construct a vector field, $\hat{\vec{n}}$, that is normal to the local roll structure. The curvature is calculated directly from the normal vector field using $c = \vec{\nabla} \cdot \hat{\vec{n}}$, and the wavelength is determined with subpixel resolution by scanning the image along the normal vector and finding the distance between the nearest peak and trough. These algorithms are similar to those used by Heutmaker *et al.* in a study of pure fluid convection patterns [10].

The transition is observed as follows. A suitable pattern is first created by allowing a TW state to develop, then freezing the pattern by suddenly setting r well above r^*. The pattern is then allowed to anneal for several days. There is an initial stage of the evolution in which the pattern changes rapidly, before relaxing toward a more ordered, quasistable configuration, although slow but persistent movement of the pattern continues to occur [11]. The measurements described below are made during this latter period of slow evolution, over a time interval that is short compared with the characteristic pattern evolution time. The nature of the resulting pattern, shown in Fig. 2, is largely determined by focus singularities at the edges of the cell, which create large areas of nearly concentric rolls, and by concave disclinations embedded in the pattern [12].

In Fig. 2(a), the convection pattern is shown at a Rayleigh number of 3.7. As the Rayleigh number is gradually reduced to a value of 1.7, just above the TW transition at r^*, the broad areas of concentric rolls, characterized by fairly uniform curvature, break up into domains of straight rolls connected by sharply angled sections, as shown in Fig 2(b). The preferred wave number at $r = 1.7$ is slightly larger than at $r = 3.7$, and several new rolls are created, either emerging from the foci, or being created by the climb of dislocations, but the final state is topologically equivalent to the initial state. The local curvature, $\vec{\nabla} \cdot \hat{\vec{n}}$, shown in Figs. 2(c) and 2(d), clearly reveals the transition between the curved texture and the angular texture, in which the boundaries between domains of straight rolls appear as bright lines of intense curvature. The local wave-number maps in Figs. 2(e) and 2(f) reveal

dark patches of wave-number frustration that are visible near the embedded defects at $r = 3.7$, which disappear at $r = 1.7$.

IV. FREE ENERGY DESCRIPTION

A rigorous treatment of this transition would have to be described in terms of the stability of instability of the various roll configurations. A more workable framework is provided by the idea of a free energy functional which determines the preferred texture of the pattern. In analogy with equilibrium thermodynamics, various attributes of the texture are assigned a free energy, and the texture with the lowest value of the total free energy is preferred. In general, there is no reason to believe that such a free energy can be found to describe a nonequilibrium pattern, but in cases such as stationary convection, where the dynamics of the patterns is basically relaxational, such a description has been successful [10]. Adopting this approach, we assume that the free energy functional may be written as the sum of three terms,

$$\mathcal{F} = \mathcal{F}_{defect} + \mathcal{F}_{boundary} + \mathcal{F}_{bulk}. \tag{5}$$

In our case, the boundary and defect terms need not be considered, because the defect structure and the roll orientation near the boundary are not changed by the transition. A description of the transition must therefore be found in the bulk term.

We proceed by analogy with the Swift-Hohenberg (SH) model, which is widely used to describe stationary convection. In this system, the partial differential equation is defined in terms of a functional derivative of $\mathcal{F}$,

$$\frac{\partial \psi}{\partial t} = -\frac{\delta \mathcal{F}}{\delta \psi}, \tag{6}$$

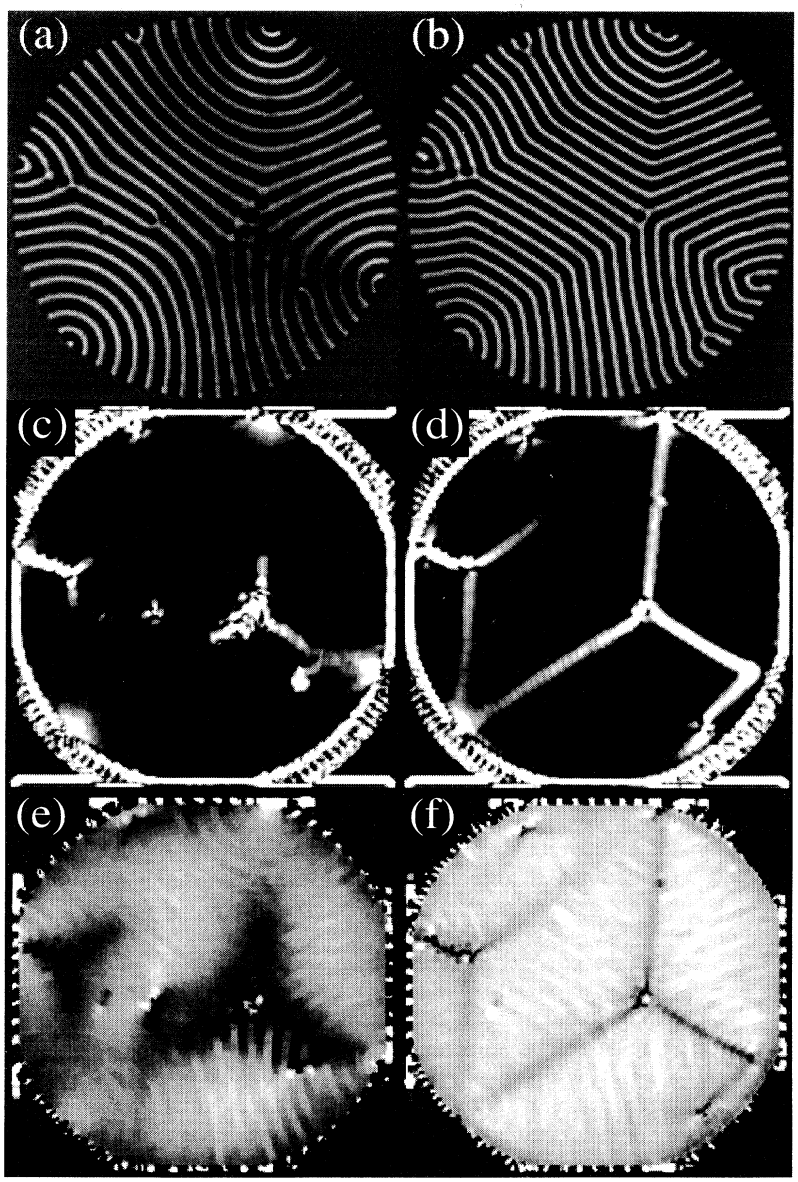

FIG. 2. Convection pattern at (a) $r = 3.7$ and (b) $r = 1.7$, the local curvature at (c) $r = 3.7$ and (d) $r = 1.7$ (white indicates the maximum curvature) and the local wave number at (e) $r = 3.7$ and (f) $r = 1.7$ (white indicates the maximum wave number).

where $\mathcal{F}$ is a functional of the order parameter, ψ, and is defined by

$$\mathcal{F} = -\int dA \left(\frac{\epsilon\psi^2}{2} - \frac{\psi^4}{4} - \left[\left({q_o}^2 + \nabla^2 \right) \psi \right]^2 \right). \quad (7)$$

Evaluation of the functional derivative gives the familiar Swift-Hohenberg equation,

$$\frac{\partial \psi}{\partial t} = \epsilon\psi - \psi^3 - \left({q_o}^2 + \nabla^2 \right)^2 \psi. \quad (8)$$

Within the context of this model, is has been proven that

$$\frac{\partial}{\partial t} \int \mathcal{F}(\psi)\, dA \leq 0, \quad (9)$$

so that the functional $\mathcal{F}$ always decreases during evolution under Eq. (6) and plays the roll of a free energy. In this case, a stable pattern must satisfy the condition that $\mathcal{F}$ is minimum, and convection texture can be predicted by looking for configurations that optimize $\mathcal{F}$. In the limit that the amplitude of the pattern is slowly varying, it is possible to recast Eq. (7) in a form that is very convenient for application to experimental patterns. By making use of the substitution,

$$\psi = |A|\, e^{i\phi} + \text{c.c.} \quad (10)$$

$$\vec{\nabla}\phi = (q_o + \delta q)\, \hat{\vec{n}}, \quad (11)$$

it was shown by Cross [3] that the bulk free energy takes the form

$$\mathcal{F}_{bulk} = \epsilon \int dA \left[\frac{1}{4} \left(\vec{\nabla} \cdot \hat{\vec{n}} \right)^2 + (\delta q)^2 \right]. \quad (12)$$

This expression, whose validity has been established for pure fluid convection patterns [10], is especially attractive because the free energy is separated into individual terms depending on curvature and wave number.

The angular transition is essentially a transition from a state in which curvature is optimized (the curved texture) to a state in which the wave number is optimized (the angular texture), and it could be interpreted as a transition from a curvature-dominated free energy to a wave-number-dominated free energy. Adopting this ansatz, we depart from the SH model by assuming that the bulk free energy is composed of the curvature and wave number terms of the SH model, but that the coefficients can be varied independently. The two terms are

$$\mathcal{F}_{curvature} = A \int \left(\vec{\nabla} \cdot \hat{\vec{n}} \right)^2 dA = A I_c, \quad (13)$$

$$\mathcal{F}_{wave\ number} = B \int (k - k_0)^2\, dA = B I_k. \quad (14)$$

The integrals I_c and I_k are the curvature and wave-number frustration, and A and B are unknown constants which in the SH model would satisfy $A = B/4 = (r-1)/4$. This modification of the free energy is not consistent with the simple structure of the SH equation, Eq. (8) above, but is introduced in an attempt to capture the trade-off between curvature and wave number that is observed in the transition.

Considering these two terms, the effect of I_k is to reward the pattern for minimizing the rms deviation of its wave number from the optimum value. Since the observed pattern has adequate mechanisms for wave-number adjustment, we can accurately estimate this value by calculating the second moment of the measured wave-number distribution. The effect of I_c is more subtle. Since the total winding angle of each roll is fixed by its perpendicular attachment to the boundary, the integral of $\vec{\nabla} \cdot \hat{\vec{n}}$ along each roll is the same in the angular and curved textures, and equal to this angle. Under this constraint, the integral of $(\vec{\nabla} \cdot \hat{\vec{n}})^2$ is minimized for uniform curvature along each roll. The presence of concave disclinations in the pattern sets up a competition between the two terms. If the rolls remain smoothly curved in the vicinity of the defects, a substantial wave-number deformation is created, as illustrated on the right-hand side of Fig. 3. To eliminate the wave-number deformation, the rolls must crawl into the corners created by the defect, as shown on the left-hand side of Fig. 3, producing lines of intense curvature emanating from the defect [13].

In Figs. 4(a) and 4(b), the distribution of the curvature and wave number are shown for a single roll both in the curved texture at $r = 3.7$, and in the angular texture at $r = 1.7$. In the curved texture, the curvature is broadly distributed below 0.1, reflecting the approximately circular shape of the rolls. In the angular state, the peak has shifted to zero curvature, reflecting the areas of straight rolls, and a long tail at large curvature is present, reflecting the narrow lines of intense curvature. Averaged over the entire pattern, the mean value of the curvature is conserved to within 10%, but the mean value of I_c increases by a factor of 2.

Considering the wave-number distribution in Fig. 4(b), the broad distribution observed in the curved state narrows substantially and shifts upward in the angular state. Averaged over the entire pattern, I_k decreases by a factor of 2.5. Evidently, in the angular state, the pattern has chosen to optimize the wave number at the expense of curvature.

In Fig. 5(a), we show the two frustration integrals, I_c and I_k, as measured during a different run on the same pattern shown in Fig. 2. In this case, r was gradually increased from 1.7 to 3.7 during a period of 60 min. and the frustration integrals were evaluated each minute. It takes about 5 min. for the pattern to react to a change in r, so there is probably an offset of 0.2 in r due to slewing in these curves. The necessity of completing the protocol

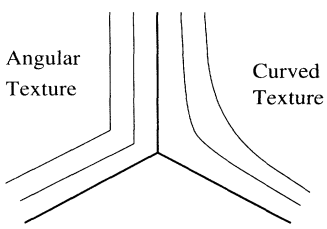

FIG. 3. Illustration of the deformation of rolls near a concave disclination.

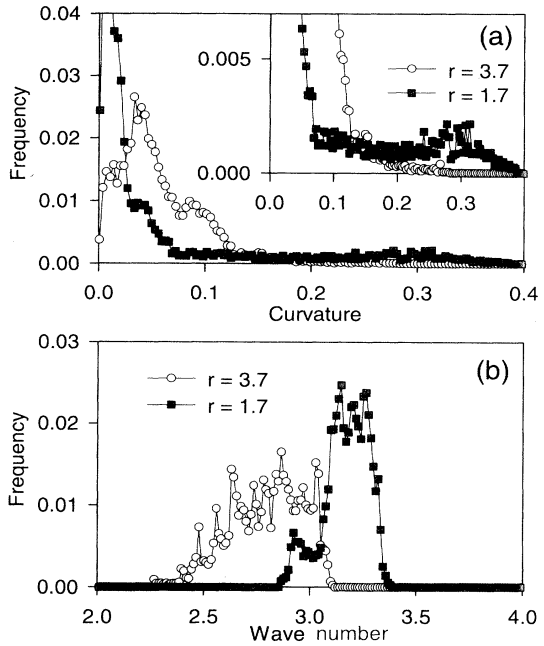

FIG. 4. Histograms of (a) curvature and (b) wave number. The data shown are integrated over a typical roll pair for both curved ($r = 3.7$) and angular ($r = 1.7$) states. Distances are scaled by the cell height.

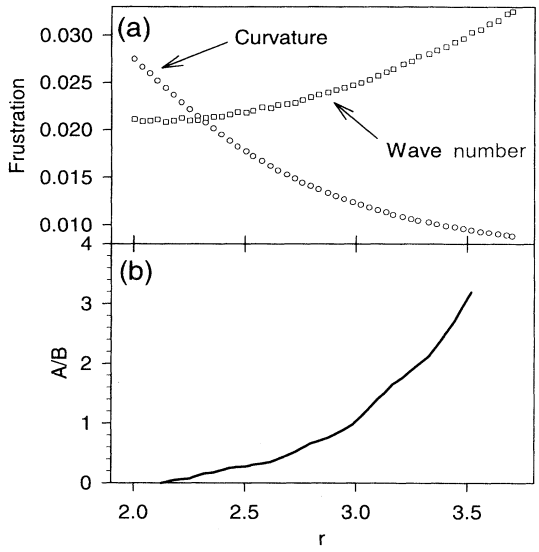

FIG. 5. (a) Curvature and wave-number frustration integrals, I_c and I_k, are shown as a function of r. (b) The ratio A/B calculated from the data in (a).

before the defect structure of the pattern has changed prevents the use of a slower slewing rate.

Using the dependence of I_c and I_k on the Rayleigh number, it is possible to estimate the ratio of the two coefficients introduced in Eqs. (13) and (14) as follows. It has been confirmed that the curved-to-angular transition is reversible and that the evolution of the roll contours from curved texture to angular texture is a one parameter family of curves. Therefore, the free energy functional can be considered to be a simple function of some geometrical deformation parameter, and at a given Rayleigh number, this free energy *function* is minimized for the observed deformation. In terms of this as yet undefined deformation parameter, ν, we can write the bulk free energy as

$$\mathcal{F}_{bulk} = AI_c(\nu) + BI_k(\nu). \tag{15}$$

By applying the condition that $\mathcal{F}_{bulk}$ is minimized for some value of the deformation, ν_0, we obtain

$$\frac{A}{B} = \frac{\partial I_k}{\partial \nu}\frac{\partial \nu}{\partial I_c} = \frac{\partial I_k}{\partial I_c}(\nu_0), \tag{16}$$

regardless of how we parameterize the deformation. The equation specifies the value of A/B, which is required for $\mathcal{F}_{bulk}$ to attain its minimum at ν_0. Since there is a one-to-one mapping between the observed patterns and the Rayleigh number, $\nu = \nu(r)$, and so r is a suitable deformation parameter. The ratio A/B can therefore be found as a function of r by differentiating the two curves shown in Fig. 5(a) with respect to r and dividing. The result of this calculation is shown in Fig. 5(b). As expected, the analysis indicates a smooth transition from a curvature-dominated free energy at high Rayleigh number to a wave-number-dominated free energy at low Rayleigh number. The value of A/B attains the SH value of $1/4$ at $r = 2.5$, and becomes equal to zero at $r = 2.0$ (or $r \approx 1.8$, if the slewing shift is included), indicating a dramatic increase in the wave-number rigidity in the angular state.

The transition described above can be described by the bulk energy term because the defect structure is stable for $1.7 < r < 3.7$. At such high Rayleigh numbers, the evolution of the defect structure probably cannot be described by a free energy. The separation of time scales between the defect evolution, which takes place over many hours, and the bulk deformation of the pattern, which occurs over a few minutes, make it possible to isolate the bulk properties. In effect, the bulk deformation plays the roll of a fast slave mode to the more slowly moving defect structure.

V. ASSOCIATION OF THE ANGULAR TRANSITION WITH THE TW STATE

In the 8% ethanol mixture, the transition to the angular texture occurred as r approached r^*, the Rayleigh number where the transition to TW convection occurs. In order to confirm that the angular state is in fact related to the TW state, experiments were done in a 1% mixture and in pure water. In the 1% mixture $\psi = -0.06$, and the transition to TW convection occurs at a much lower value of r at a smaller convection amplitude (see Fig. 1). The Prandtl number of the 1% mixture is equal to 6.5, which is not significantly different from pure water. Data taken in the 1% mixture is shown in Fig. 6. The texture of the convection pattern remains curved down to $r = 1.4$, shown in Fig. 6(a), but the transition to the angular texture occurs $r = 1.2$, which is just above r^* in the 1% mixture. The interpretation of the transition is not as clear in this case because it occurs in a small amplitude state near onset, where the defect structure is much

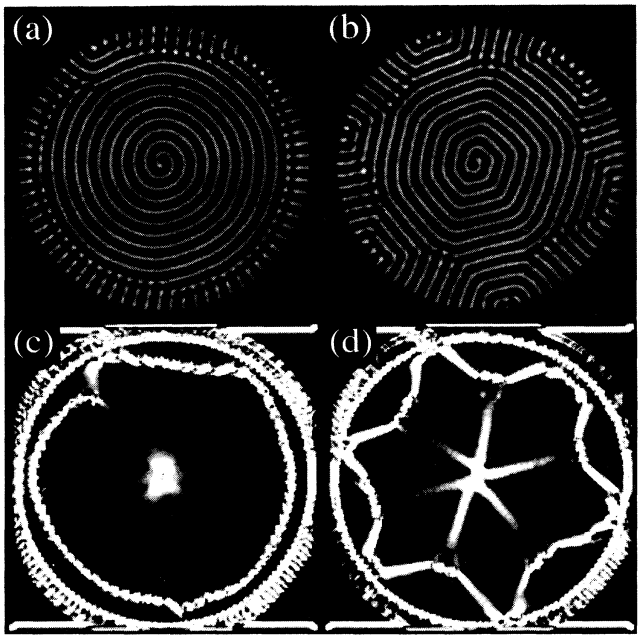

FIG. 6. Patterns in a 1% ethanol-water mixture at (a) $r = 1.4$, and (b) $r = 1.2$, and the local curvature at (c) $r = 1.4$, and (d) $r = 1.2$.

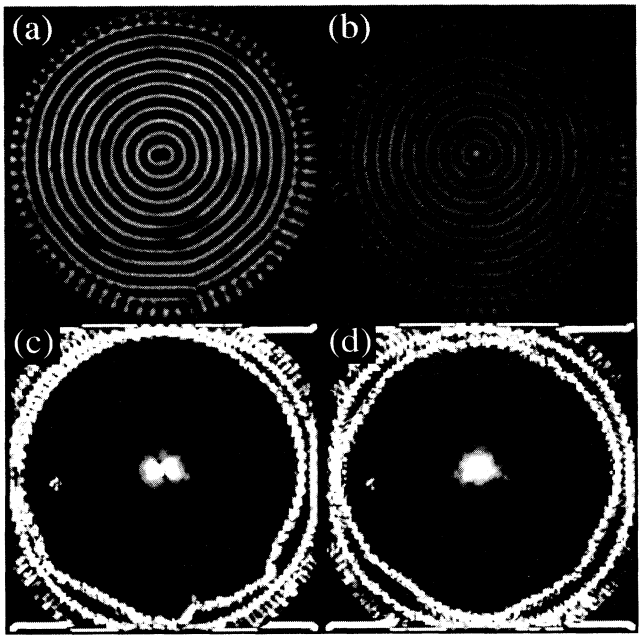

FIG. 7. Patterns in pure water at (a) $r = 1.4$, and (b) $r = 1.05$, and the local curvature at (c) $r = 1.4$, and (d) $r = 1.05$.

more plastic. In this case, the concave disclinations that cause wave-number frustration form in the course of the transition to the angular texture. This suggests that the defect contribution to the free energy varies significantly with r, making it impossible to separate bulk from defect effects.

Finally, the experiment was repeated with pure water, which does not support TW convection, with the results shown in Fig. 7. The pure fluid manifests a curved texture in Fig. 7(a), which is identical to that seen in the 1% mixture, but as the Rayleigh number is gradually reduced, there is no hint of an angular texture, even as r goes below onset and the pattern fades away. Figure 7(b) shows the persistence of the curved texture at $r = 1.05$, where the amplitude of convection is so small as to make visualization difficult.

The fact that the angular texture is associated with the transition to TW convection is strongly supported by this series of experiments. The transition occurs as $r \to r^*$ at two different values of ψ, even though the value of r^* is very different in the two cases. In addition, the angular texture does not occur in pure water, which has a Prandtl number identical to that of the 1% mixture and only differs from the mixture in that it does not support a TW convection state.

There is experimental evidence that the transition does result from a competition between wave number and curvature frustration, and not from an intrinsic instability of curved rolls. In the 8% mixture, regions of curved rolls have been observed to coexist with the angular texture in cases where there are regions of the pattern that are free from disclinations and other defects that bring about a competition between curvature and wave-number frustration. Apparently, even in the angular texture curved rolls are preferred over angular rolls unless the wave-number optimization suffers.

VI. NUMERICAL OPTIMIZATION OF THE FREE ENERGY

In Sec. IV above, the relative weight of the wave-number and curvature frustration terms in the effective free energy was calculated, based on the assumption that the two terms that are present in the SH model are sufficient to capture the essence of the transition. It would be of interest to confirm that the transition does follow from this form of the free energy functional by searching for the minimum energy pattern as a function of A/B. This is not practical, because the convection pattern is a continuous field having an infinite number of degrees of freedom, and a discrete representation of the pattern with sufficient resolution to represent the transition would require $\sim 10^5$ degrees of freedom. However, if the convection pattern is represented as a series of lines corresponding to the roll boundaries, an adequate representation of the pattern may be obtained from a much smaller number of degrees of freedom. It is then possible to search for a configuration that minimizes the free energy functional, which can easily be evaluated in the simplified system.

In order reproduce the transition, the simplest possible geometry was chosen; that of a single concave disclination at the center of a triangular convection cell. The pattern is composed of concentric rolls centered on the three vertices of the triangle, and the required perpendicular attachment of the rolls to the cell boundary is easily fulfilled, so that the only source of frustration in the pattern is the disclination at the center. The roll contours surrounding each of the three vertices are specified in polar coordinates by 32 points, so that an arbitrary

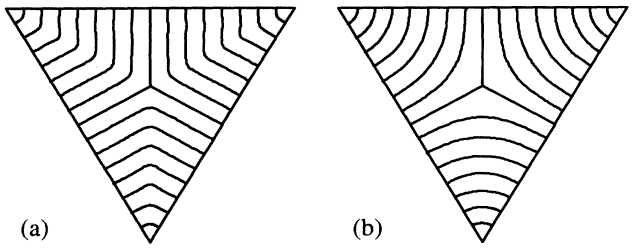

FIG. 8. Roll contours of the minimum energy configurations of the postulated free energy (a) with $A/B = 0.1$, and (b) with $A/B = 10$.

roll configuration may be specified, except for the constraint that the rolls are attached to the cell boundary. Efficient searching of the configuration space is accomplished by using a simplex search algorithm to vary the Fourier modes of the roll contour functions, $R(\theta)$, including a zero-frequency term that specifies each roll's mean distance from the vertex. A variety of other search strategies were tried that converged to the same optimum configuration with varying degrees of efficiency.

In Fig. 8(a) the optimum pattern configuration is shown for $A/B = 0.1$, which corresponds to the angular texture, and in Fig. 8(b) the configuration is shown for for $A/B = 10$, which corresponds to the curved texture. The roll contours in the simulations of both the angular texture and the curved texture are similar in appearance to the experimental patterns, with lines of intense curvature in Fig. 8(a) and broad regions of even curvature in Fig. 8(b). A detailed comparison of the computer simulation with the observed contours reveals small discrepancies in the roll shapes, particularly in the curved texture. These discrepancies can be reduced by adding a small term proportional to $(\delta q)^4$ to the wave-number frustration integral.

VII. CONCLUSION

In this paper, we have reported a reversible transition between a curved texture, generic to Rayleigh-Bénard convection, and an angular texture, in which the pattern breaks up into geometric domains of straight rolls. By isolating the bulk properties of the pattern and introducing an effective free energy containing separate terms sensitive to wave-number and curvature, we have been able to describe the transition in terms of a competition between wave-number and curvature optimization. The angular texture seems to be closely related to the distinctive geometric domains of straight rolls that are observed in stripe domains in ferromagnetic garnets, which suggests that the primary difference between the stripe domain patterns and conventional convection patterns is an extraordinary wave-number rigidity in the angular stripe domain patterns. It would be interesting to see if the wave-number distribution in the stripe domain patterns is in fact narrower than would be expected from the generic Swift-Hohenberg model.

The transition in texture appears to be closely associated with the transition between stationary convection and traveling-wave convection. In the stationary convection regime, the Swift-Hohenberg equation is thought to be applicable, whereas several complex generalizations of the Swift-Hohenberg equation have been proposed as models for traveling-wave convection [14,15]. The presence of the angular texture near the transition may provide additional information about the bifurcation to traveling waves, about which very little is known. Unfortunately, the modification of the Swift-Hohenberg free energy functional that we have introduced upsets the local rotational invariance of the model, and therefore it is not straightforward to derive a partial differential equation from this functional. Nevertheless, the requirement that an angular texture is present at the bifurcation point may constrain the structure of traveling-wave models.

ACKNOWLEDGMENTS

We are happy to thank Alan Newell, who first called our attention to the importance of this transition. We would also like to acknowledge Mike Cross and Doug Ridgway for useful discussions. This work was supported by the U. S. Department of Energy under Grant No. DE-FG03-90ER14148.

[1] P. Manneville, *Dissipative Structure and Weak Turbulence* (Academic Press, Boston, 1990).
[2] M. C. Cross and P. C. Hohenberg, Rev. Mod. Phys. **65**, 851 (1993).
[3] M. C. Cross, Phys. Rev. A **25**, 1065 (1982).
[4] J. Swift and P. C. Hohenberg, Phys. Rev. A **15**, 319 (1977).
[5] M. Seul, L. R. Monar, L. O'Gorman, and R. Wolf, Science **254**, 1616 (1991).
[6] R. W. Walden, P. Kolodner, A. Passner, and C. M. Surko, Phys. Rev. Lett. **55**, 496 (1985).
[7] M. Lücke, W. Barten, and M. Kamps, Physica D **61**, 183 (1992).
[8] W. Barten, M. Lücke, W. Hort, and M. Kamps, Phys. Rev. Lett. **63**, 376 (1989).
[9] K. D. Eaton *et al.*, Phys. Rev. A **43**, 7105 (1991).
[10] M. S. Heutmaker, P. N. Fraenkel, and J. P. Gollub, Phys. Rev. Lett. **54**, 1369 (1985).
[11] G. Ahlers, D. S. Cannell, and V. Steinberg, Phys. Rev. Lett. **54**, 1373 (1985).
[12] A. C. Newell, T. Passot, and J. Lega, Annu. Rev. Fluid Mech. **25**, 399 (1993).
[13] It is tempting to call these lines of intense curvature domain walls. This is not appropriate in the context of Cross's analysis [3] because the energy associated with a domain wall is assumed to arise from suppression of the convective amplitude, which is not observed for $r \gg 1$.
[14] M. Bestehorn, R. Friedrich, and H. Haken, Z. Phys. B **75**, 265 (1989).
[15] I. Aranson and L. Tsimring, Phys. Rev. Lett. **75**, 3273 (1995).

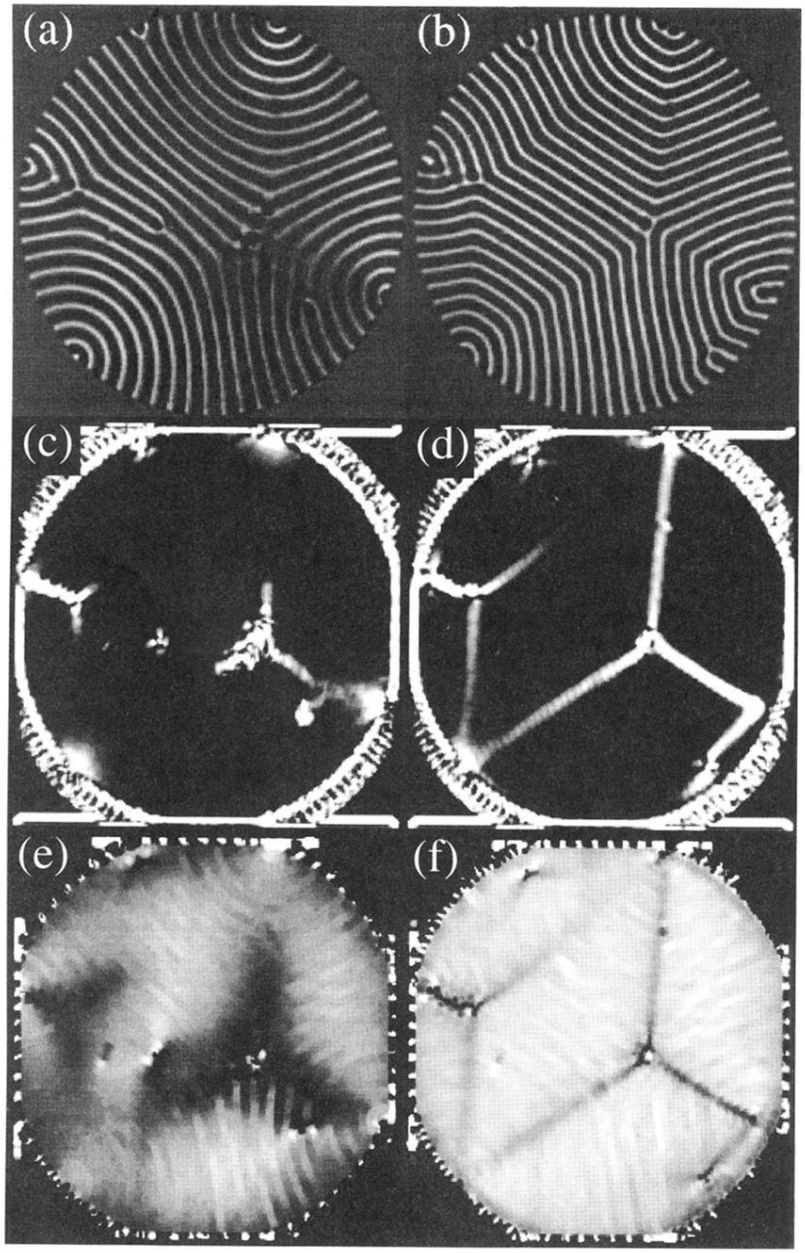

FIG. 2. Convection pattern at (a) $r = 3.7$ and (b) $r = 1.7$, the local curvature at (c) $r = 3.7$ and (d) $r = 1.7$ (white indicates the maximum curvature) and the local wave number at (e) $r = 3.7$ and (f) $r = 1.7$ (white indicates the maximum wave number).

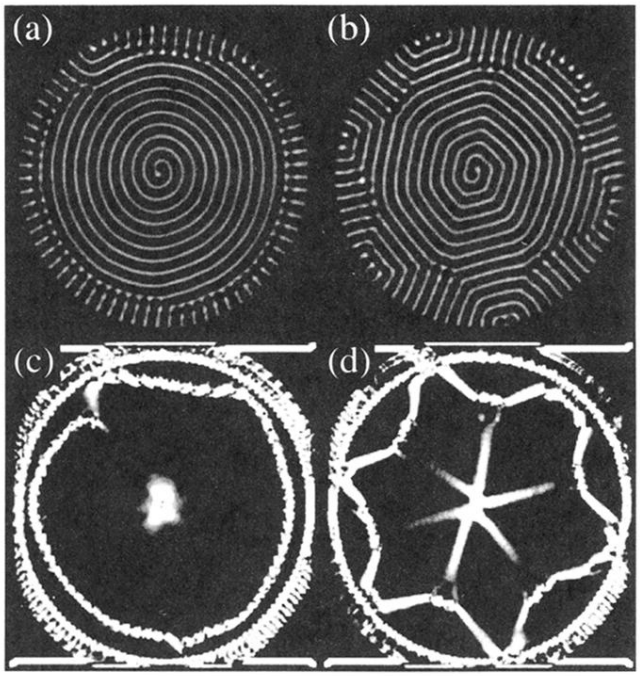

FIG. 6. Patterns in a 1% ethanol-water mixture at (a) $r = 1.4$, and (b) $r = 1.2$, and the local curvature at (c) $r = 1.4$, and (d) $r = 1.2$.

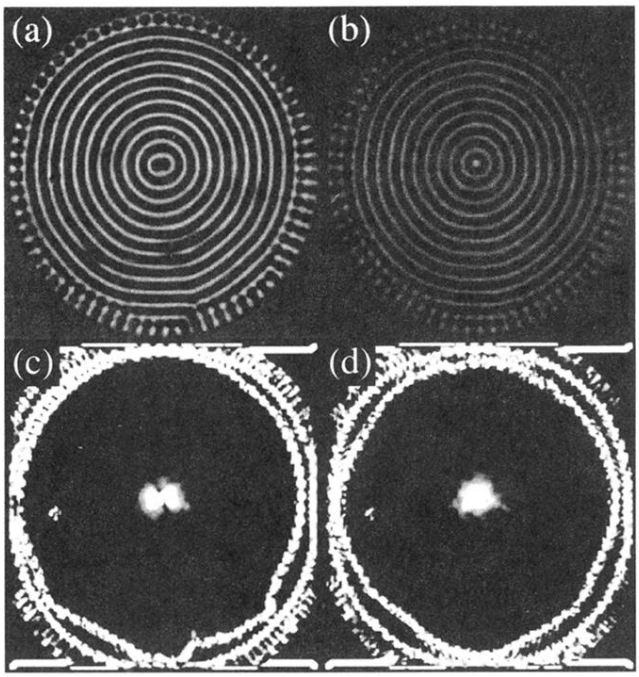

FIG. 7. Patterns in pure water at (a) $r = 1.4$, and (b) $r = 1.05$, and the local curvature at (c) $r = 1.4$, and (d) $r = 1.05$.